INTERNATIONAL JOURNAL FOR NUMERICAL METHODS IN FLUIDS
Int. J. Numer. Meth. Fluids 2006; **51**:913–936
Published online 4 January 2006 in Wiley InterScience (www.interscience.wiley.com). DOI: 10.1002/fld.1165

SPH computation of plunging waves using a 2-D sub-particle scale (SPS) turbulence model

Songdong Shao*,†,§ and Changming Ji‡,¶

Research Institute of Water Resources and Hydro-electric Engineering, North China Electric Power University, Zhuxinzhuang, Deshengmenwai, Beijing 102206, China

SUMMARY

The paper presents a 2-D large eddy simulation (LES) modelling approach to investigate the properties of the plunging waves. The numerical model is based on the smoothed particle hydrodynamics (SPH) method. SPH is a mesh-free Lagrangian particle approach which is capable of tracking the free surfaces of large deformation in an easy and accurate way. The Smagorinsky model is used as the turbulence model due to its simplicity and effectiveness. The proposed 2-D SPH–LES model is applied to a cnoidal wave breaking and plunging over a mild slope. The computations are in good agreement with the documented data. Especially the computed turbulence quantities under the breaking waves agree better with the experiments as compared with the numerical results obtained by using the k–ε model. The sensitivity analyses of the SPH–LES computations indicate that both the turbulence model and the spatial resolution play an important role in the model predictions and the contributions from the sub-particle scale (SPS) turbulence decrease with the particle size refinement. Copyright © 2006 John Wiley & Sons, Ltd.

KEY WORDS: SPH; 2-D LES; particle scale (PS); sub-particle scale (SPS); numerical phase-averaging; plunging wave

INTRODUCTION

The breaking waves are of great engineering interest because of the tremendous forces they exert on the coastal structures and their ability to transport large quantities of the sediment

*Correspondence to: S. Shao, Research Institute of Water Resources and Hydro-electric Engineering, North China Electric Power University, Zhuxinzhuang, Deshengmenwai, Beijing 102206, China.
†E-mail: songdongshao@hotmail.com
‡E-mail: cmji@ncepubj.edu.cn
§Associate Professor.
¶Professor and Director.

Contract/grant sponsor: National Natural Science Foundation of China; contract/grant number: 50579019

Received 27 July 2005
Revised 10 November 2005
Accepted 12 November 2005

and drastically reshape the coastal bathymetry. The wave breaking is generally classified as the spilling, plunging and surging, with a gradual transition between each regime [1]. In most natural beaches, the commonly observed wave breaking types are the spilling and plunging breakers, in which the latter display especially spectacular phenomena. When the wave plunges, the wave crest curls downwards and impinges on the wave trough in the front, trapping a large amount of the air entrainment. Meanwhile, the wave breaking process generates the turbulence and vorticity, which are very important for the solute transport and sediment mixing in the surf zone [2].

The wave breaking processes must be clarified in order to solve many coastal problems. However, the study of breaking waves is a very difficult task for a number of reasons. The breaking waves experience the rapid wave shape deformation and fast energy dissipation. The flows change the regime from the irrotational to rotational, accompanied by the generations of strong turbulence. The laboratory experiments and field observations have the measurement difficulties and are also limited by the site and environmental conditions. Thus the numerical studies of the breaking wave are becoming increasingly popular since they can provide the flow details without scaling and observational constraints. The flow in the waves is generally treated as irrotational before the wave breaking and the potential flow theory [3] can be used with enough accuracy. However, during and after the wave breaking, the flow becomes highly rotational and complex, thus necessitating the implementation of more general descriptions of the wave dynamics [4]. The most appropriate way to investigate the breaking waves in the surf zone might be the employment of the fundamental hydrodynamic equations such as the Navier–Stokes (N–S) equations or Reynolds averaged N–S (RANS) equations. They are capable of calculating the flows inside the complex geometries to disclose very refined information about the velocities, turbulence, transport properties, etc. For example, Lemos [5] simulated a periodic wave breaking on the sloping bed and Takikawa *et al.* [6] studied the breaking wave transformation over a slope using both the experimental and numerical analyses. Lin and Liu [2, 7] made the quantitative comparisons between the spilling and plunging breakers by using an advanced RANS modelling and an excellent agreement was found between the numerical and experimental results.

The turbulence modelling is one of the key issues in the study of breaking waves. The RANS equations with different turbulent closures have been widely used for the study. The turbulent stresses in the RANS equations can be closed using any of the existing turbulence models. No single turbulence model is accepted universally for solving all the problems but each model has some advantages over the other depending on the type and nature of the flows and the desired accuracy of the results. The most commonly used turbulent closure up-to-date could be the two-equation k–ε model that solves two separate transport equations to determine the turbulence kinetic energy and its dissipation rate. For example, Bradford [8] used the classical and improved k–ε models and Lin and Liu [2, 7] employed the non-linear k–ε formulations in the studies of the wave breaking. It is worth mentioning here that the Reynolds stress model (RSM) also provides the closure of RANS equations by solving several transport equations. It is considered to be superior to k–ε like models in simulating the complex flows but it requires the extensive computational effort and time.

However, both Lemos [5] and Lin and Liu [2, 7] found that the turbulence levels at wave breaking were numerically overestimated. In the surf zone, the computed turbulence

intensities were generally about 25–50% higher than the measured values. According to the summary review of Christensen *et al.* [9], the turbulence levels within the surf zone were overestimated in all the reported studies using the RANS approach. The overestimation of turbulence could be attributed to the following reasons. First, the traditional turbulent closure models cannot accurately predict the initiation of turbulence in a rapidly distorted shear flow region such as in the initial stage of wave breaking. Second, the coefficients used in the closure models were obtained from the experiments for the steady flows rather than the oscillatory flows [10]. Besides, the influence of air bubbles entrained in the breaking waves is also quite dominant. In view of these uncertainties, more advanced turbulence modelling approaches, such as the large eddy simulation (LES), should be considered to investigate the turbulence properties under the breaking waves.

The LES lies between the extremes of the direct numerical simulation (DNS) and RANS modelling and attempts to capture the large-scale motion, which is thought to contain most of the energies and momentums. Thus eddies capable of being resolved by the computational grid are allowed to evolve following the governing equations and a model is employed to represent the turbulence at the sub-grid scale (SGS). The N–S equations are averaged over the grid volume by a spatial filter and the unknown stresses are produced related to the SGS motion. Watanabe and Saeki [11] employed an improved SGS turbulence model based on the re-normalization group theory to study the 3-D characteristics of breaking waves using the CIP approach. Christensen and Deigaard [12] used a 3-D Smagorinsky model [13] to investigate the detailed turbulence structures under different wave breakers. The 2-D LES modelling cannot be the real LES, since the simulation of eddies is in a two-dimensional plane and the stretching of eddies which are representative of the true turbulence cannot be adequately disclosed. In spite of the uncertainties and concerns, the 2-D LES modelling has already shown its robustness [9]. For example, a 2-D LES model used by Zhao and Tanimoto [14] gave quite promising indications of such a modelling approach. Besides, Gotoh *et al.* [15] employed a 2-D sub-particle scale (SPS) turbulence model using the moving particle semi-implicit (MPS) solver [16] to simulate a turbulent jet. The essential unsteady behaviours of the jet and the mixing processes were well predicted by the model.

This paper aims to use the 2-D SPS turbulence model of Gotoh *et al.* [15] to investigate the plunging wave breaking over a mild slope. The numerical model was developed from the smoothed particle hydrodynamics (SPH) method [17]. SPH is a pure mesh-free Lagrangian particle approach which was originally developed for the astrophysics and later applied to the fluid flows [18]. It has proved to be a robust method for tracking the free surfaces of large deformation such as the breaking waves. Recently an incompressible version of the SPH algorithm was established and employed to the applications of the solitary wave breaking on a beach [19], the cnoidal waves breaking over a slope [20] and the regular waves overtopping of a sloping seawall [21], where the two equation k–ε model was used as the turbulent closure. In the following sections, the incompressible SPH method will be coupled with the LES turbulence modelling and the computations will be compared with the experimental data of Ting and Kirby [22] and the numerical results of Lin and Liu [2] using an RANS approach. The sensitivity analyses of the incompressible SPH–LES model are made based on the numerical tests using different turbulence models and spatial resolutions represented by the particle spacing.

GOVERNING EQUATIONS AND SOLUTION PROCESSES

The Lagrangian form of the N–S equations is employed for the SPH model

$$\frac{1}{\rho}\frac{\mathrm{D}\rho}{\mathrm{D}t} + \nabla \cdot \mathbf{u} = 0 \tag{1}$$

$$\frac{\mathrm{D}\mathbf{u}}{\mathrm{D}t} = -\frac{1}{\rho}\nabla P + \mathbf{g} + v_0 \nabla^2 \mathbf{u} \tag{2}$$

where ρ is the density, t the time, $\mathbf{u}$ the velocity, P the pressure, $\mathbf{g}$ the gravitational acceleration, and v_0 the laminar kinematic viscosity. It is noted that the mass conservation equation (1) is written in the form of a compressible flow. The incompressibility of the flow is enforced by setting $\mathrm{D}\rho/\mathrm{D}t = 0$ at each fluid particle during the incompressible SPH computations.

The LES mass and momentum equations of the particle-scale (PS) flow are derived through the filtering operations of the above N–S equations, similar to the conception and formulations employed in an Eulerian LES. By using a spatial filter on Equations (1) and (2) and neglecting the Leonard and Cross terms, the following equations for the PS flow are derived:

$$\frac{1}{\rho}\frac{\mathrm{D}\rho}{\mathrm{D}t} + \nabla \cdot \bar{\mathbf{u}} = 0 \tag{3}$$

$$\frac{\mathrm{D}\bar{\mathbf{u}}}{\mathrm{D}t} = -\frac{1}{\rho}\nabla \bar{P} + \mathbf{g} + v_0 \nabla^2 \bar{\mathbf{u}} + \frac{1}{\rho}\nabla \cdot \vec{\bar{\tau}} \tag{4}$$

where '$-$' denotes the PS component and $\vec{\bar{\tau}}$ is the sub-particle scale (SPS) stress tensor with each element defined by

$$\tau_{ij} = \rho(\overline{u_i u_j} - \overline{u_i}\,\overline{u_j}) \tag{5}$$

which should be modelled using an appropriate turbulent closure.

In the incompressible SPH computations, Equations (3) and (4) are solved using a prediction–correction two-step procedure as found in References [19–21]. The first/prediction step is an explicit integration in time without enforcing the incompressibility. In Equation (4) only the stress tensor, the laminar viscosity and gravitational terms are used and an intermediate particle velocity and position are obtained. At this time, the incompressibility (or mass conservation) is not satisfied due to the particle motion, which is manifested by the deviations of the instantaneous particle density from the initial reference density. Therefore, in the second/correction step, the pressure gradient term is used to update the particle velocity and position obtained from the prediction step, so as to satisfy the incompressibility again. The pressure is calculated from the solution of a pressure Poisson equation obtained by combining the mass and momentum equations (3) and (4), which is quite similar to the formulations widely found in the grid projection method. This semi-implicit algorithm of calculating the pressures distinguishes the incompressible SPH method of Shao and Gotoh [19] from the original weakly compressible SPH approach of Monaghan [17, 18] in that the latter calculated the pressures explicitly from an equation of state assuming a large sound speed in the flows.

During the numerical simulations, the time step Δt is dynamically adjusted to improve the computational efficiency based on the Courant condition and viscous diffusion. Besides,

a particle link-list [19] is also generated in the code to search for the neighbouring interaction particles in order to reduce the CPU time.

2-D LES TURBULENCE MODELLING

Particle scale (PS) and sub-particle scale (SPS) turbulences

Similar to the Eulerian LES conception, the total turbulences k in the SPH approach are composed of the PS and SPS components. The SPS turbulence quantity k_{SPS} can be directly calculated from the SPS turbulence model and the PS turbulence quantity k_{PS} is calculated from the differences between the instantaneous velocity and the phase-averaged mean velocity. According to Gotoh *et al.* [15], a velocity series of 50–$100T$ (where T is the wave period) is usually needed to accurately estimate the PS turbulence.

Sub-particle scale (SPS) turbulence model

The concept of SPS in the SPH approach is very similar to the sub-grid scale (SGS) in the grid method in that it is employed to represent the effects of turbulence at sub-particle scales. Numerous complicated formulations have been reported to model the SGS turbulences, but a simple SGS model is still capable of providing adequate information on the scales of interest. For example, the Smagorinsky model [13] has been widely and successfully used due to its simplicity and effectiveness.

The eddy viscosity assumption (Boussinesq's hypothesis) is often used to model the SPS turbulent stresses in Equation (5) as

$$\tau_{ij}/\rho = 2\nu_{\mathrm{T}}\overline{S}_{ij} - \tfrac{2}{3}k_{\mathrm{SPS}}\delta_{ij} \tag{6}$$

where ν_{T} is the turbulence eddy viscosity, $\overline{S}_{ij}$ the strain rate of mean flow, and δ_{ij} the Kronecker delta.

The turbulence eddy viscosity ν_{T} is also calculated from the strain rate of the mean flows which have already been resolved. In this sense, the turbulence model works like a mixing length model at the SPS scale

$$\nu_{\mathrm{T}} = (C_{\mathrm{s}}\Delta X)^2|\overline{S}| \tag{7}$$

where C_{s} is the Smagorinsky constant, ΔX the particle spacing, and $|\overline{S}|$ the local strain rate defined by

$$|\overline{S}| = (2\overline{S}_{ij}\overline{S}_{ij})^{1/2} \tag{8}$$

The choice of value for C_{s} is undergoing some kinds of debate. As pointed out by Yoshizawa [23], the values of C_{s} vary from 0.1 in the channel flow to 0.12–0.14 in the mixing layer, and up to 0.23 in the decaying turbulence. Yoshizawa [23] also pointed out that some complex flows exhibit the combinations of different turbulence features and one single value of C_{s} cannot describe the flow accurately. In spite of these concerns, the present SPH simulations use a constant value of $C_{\mathrm{s}} = 0.1$, following Christensen and Deigaard [12] in their 3-D LES simulations of spilling and plunging breakers.

According to the derivations of Gotoh *et al.* [15], the SPS turbulence kinetic energy can be approximately related to the turbulence eddy viscosity by

$$v_T = C_T k_{SPS}^{1/2} \Delta X \tag{9}$$

where $C_T = 0.08$ is a turbulence constant [15] and ΔX is equivalent of the filter width. Here it should be noted that Gotoh *et al.* [15] obtained the value of C_T in a turbulent mixing layer simulation. The optimum value for the breaking waves is yet to be further investigated.

Particle scale (PS) turbulence and numerical phase-averaging

The DNS and LES are in many aspects similar to the experimental investigations with regard to the problem of distinguishing between the turbulence fluctuations and the ordered water motions [12]. In the experiment, the phase-averaging is often used when the waves are generated by a regular periodic motion of the wave generator (or by several repetitions of a short time series). The assumption is that the averaged value over a large number of waves is taken as the ordered wave motion and the deviation from the mean is taken as the turbulence fluctuation. Based on this guideline, the numerical phase-averaging approach was proposed to analyse the numerical data by Christensen and Deigaard [12].

The similar phase-averaging method is also used in this paper to extract the turbulence velocities from the instantaneous velocities computed from the SPH model. A long-time velocity series are numerically phase-averaged to get the mean velocity and the turbulence velocities are calculated as the differences between the instantaneous velocities and the phase-averaged velocity. Thus an instant velocity u or (v) is split into a phase-averaged quantity $\overline{u}$ or $(\overline{v})$ and a turbulence fluctuation u' or (v')

$$u = \overline{u} + u' \tag{10}$$

$$v = \overline{v} + v' \tag{11}$$

and the PS turbulence kinetic energy in a 2-D plane can be defined by

$$k_{PS} = \tfrac{1}{2}(\overline{u'^2} + \overline{v'^2}) \tag{12}$$

BRIEF REVIEWS OF SPH THEORY

In the SPH concept, the motion of each particle is calculated by the interactions from the neighbouring particles using an analytical kernel function. All terms in the governing equations are formulated by the particle interaction models and thus a grid is not needed in the computation. For a detailed illustration of the SPH background refer to Monaghan [17]. The SPH kernels can have many different forms and the use of different kernels is the SPH analogue of using different difference schemes in a finite difference method. By balancing the computational accuracy and efficiency, the kernel based on the spline function and normalized in 2-D [17] is widely used in various hydrodynamic applications.

In SPH computations, the particles move in a pure Lagrangian coordinates and the advection in the governing equations is directly calculated by the particle motion without the numerical diffusion, which is often reported in the Eulerian grid methods. The numerical diffusion becomes a severe problem when the deformation of free surfaces is very large such as

in case of the wave breaking. The treatment of surface cells to capture the sharpness of the free surface could become quite complicated in a grid model.

Several key SPH formulations are summarized as follows. For example, the fluid density ρ_a of particle a is calculated by

$$\rho_a = \sum_b m_b W(|\mathbf{r}_a - \mathbf{r}_b|, h) \tag{13}$$

where a and b are the reference particle and its neighbours, m_b the particle mass, $\mathbf{r}_a$ and $\mathbf{r}_b$ the positions of particles, W the interpolation kernel, and h the smoothing distance, which determines the range with which a particle interacts with the neighbouring particles.

The pressure gradient term has different forms depending on the derivation used. The following symmetric form is used since it exactly conserves the linear and angular momentums

$$\left(\frac{1}{\rho}\nabla P\right)_a = \sum_b m_b \left(\frac{P_a}{\rho_a^2} + \frac{P_b}{\rho_b^2}\right) \nabla_a W_{ab} \tag{14}$$

where the summation is over all particles other than particle a and $\nabla_a W_{ab}$ is the gradient of the kernel taken with respect to the position of particle a. Similarly, the divergence of a vector $\mathbf{u}$ and a tensor $\overrightarrow{\overrightarrow{\tau}}$ can also be formulated.

Following Shao and Gotoh [19], the Laplacian is formulated as a hybrid of a standard SPH first derivative with a finite difference approximation for the first derivative, which is good for the numerical stability and can avoid the decoupling of pressures

$$\nabla \cdot \left(\frac{1}{\rho}\nabla P\right)_a = \sum_b m_b \frac{8}{(\rho_a + \rho_b)^2} \frac{(P_a - P_b)(\mathbf{r}_a - \mathbf{r}_b) \cdot \nabla_a W_{ab}}{|\mathbf{r}_a - \mathbf{r}_b|^2} \tag{15}$$

The laminar viscosity term is formulated in the same way as the Laplacian, which is represented by

$$(v_0 \nabla^2 \mathbf{u})_a = \sum_b m_b \frac{2(v_a + v_b)}{\rho_a + \rho_b} \frac{(\mathbf{u}_a - \mathbf{u}_b)(\mathbf{r}_a - \mathbf{r}_b) \cdot \nabla_a W_{ab}}{|\mathbf{r}_a - \mathbf{r}_b|^2} \tag{16}$$

FREE SURFACES AND BOUNDARY CONDITIONS

Since the detailed treatment procedures of the free surfaces and boundary conditions have been explained in the previous works [19–21], here only two key issues are reviewed.

In the SPH computations, the free surfaces can be easily and accurately tracked by the particles without the numerical diffusion. Since no particle exists in the outer region of the free surface, the particle density on the free surfaces should drop abruptly. We give a zero pressure to each of the surface particles.

The solid boundaries such as the seabed and the inclined slope are treated by the fixed wall particles, which balance the pressure of inner fluid particles and prevent them from penetrating the wall. The pressure Poisson equation is solved on the wall particles and the Neumann boundary condition is imposed. The incident wave is produced by moving a numerical wave paddle located at the offshore boundary. It is also consisted of wall particles but they move following a prescribed motion and thus generate the desired wave series.

SPH–LES SIMULATION OF PLUNGING WAVE BREAKING

Experimental setup

The detailed experimental setup has been given in the original paper of Ting and Kirby [22]. Here some important parameters are summarized by also referring to Lin and Liu [2]. The following notations are introduced: ζ is the instantaneous water surface elevation and $\overline{\zeta} = (1/T)\int_0^T \zeta \, \mathrm{d}t$ is the time-averaged water surface elevation over one wave period. The local still water depth is represented by d and the time-averaged water depth is represented by $h = d + \overline{\zeta}$.

A sketch view of the experimental setup is shown in Figure 1, according to Ting and Kirby [22] and Lin and Liu [2]. In the figure, a mild beach with a constant slope of $s = \frac{1}{35}$ is connected to a region with a constant water depth of $d_c = 0.4$ m. The coordinate system is chosen so that the original $x = 0.0$ m is located at the position where the still water depth is $d_0 = 0.38$ m and $y = 0.0$ m is located at the still water surface. The incident cnoidal wave has a wave height $H = 0.128$ m in the constant water depth and a wave period $T = 5.0$ s. According to the laboratory records, the waves broke at $x_b/d_c = 19.49$ with the time-averaged water depth $h_b/d_c = 0.385$. The velocities and free surface displacements were measured at several vertical cross-sections on the onshore side of the breaking point. They were obtained by performing the phase average of the measured data 20 min after the first wave was generated. The turbulence velocities were extracted from the data after the mean velocities were obtained. The data measured at $(x - x_b)/h_b = 3.571,\ 6.494,\ 9.740$ and 16.883 are used here for comparisons with the SPH–LES computations and the numerical results of Lin and Liu [2] using an RANS approach. In Figure 1, these cross-sections are shown as 1, 2, 3 and 4, respectively.

Computational parameters and settings

By balancing both the computational efficiency and the accuracy, the computational domain is taken to be 18.0 m long, covering from $x/d_c = -5.0$ to $x/d_c = 40.0$. The incident wave is

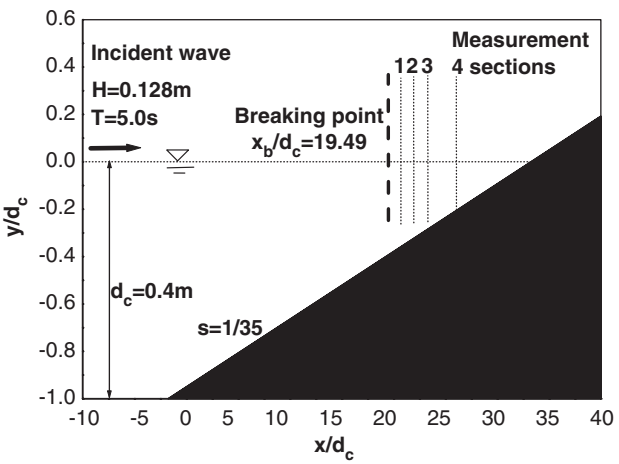

Figure 1. Sketch view of experimental setup for wave breaking [2, 22].

generated by moving a numerical wave paddle at the entrance of the computational domain. The reflections from the downstream slope are quite small in this case and can be ignored. According to the estimations of Christensen *et al.* [24], the wave reflection coefficient was 0.008 and thus less than 0.01% of the incoming wave energy was reflected. The time step Δt is automatically adjusted in the computation. The initial particle spacing is chosen as $\Delta X = 0.02$ m and approximately 10 000 particles are employed in the SPH computations. The fluid particles are initially arranged on a regular and equally spaced grid system, with the boundary particles added to form the slope and the offshore wave maker.

Number of phase-averaged waves and convergence discussions

In order to understand how the numerical results are different when different numbers of the waves are used in the phase-averaging process, we made an investigation on the convergence of the results in terms of the number of waves being phase-averaged. The SPH model was run for 100 wave periods and the phase-averaging of data was made using 20–90 waves. The first 10 waves were discarded and not used in the phase-averaging since the computed waves in the surf zone have not yet reached the fully steady state.

Based on the data analyses, it was found that there were only slight changes in the wave surface profiles if the number of waves being phase-averaged was more than 30. However, as for the turbulence quantities, the number of phase-averaged waves needs to be at least 40 in order to get the stable solution. By considering the accuracy of results and CPU time, 60 waves will be employed to perform the phase-averaging in the following sections to interpret all the numerical data. The main computations using a particle spacing $\Delta X = 0.02$ m (equivalent of particle numbers being 10 000) can be finished within 60 hours by a CPU 2.99 GHz and RAM 1.0 GB PC.

Uncertainties of 2-D LES modelling

Strictly speaking, a 2-D sub-particle scale turbulence model cannot treat 3-D turbulence flows like the breaking waves in a very accurate way. As shown in the later sections of the paper, the resolved turbulence kinetic energy is more significant than the modelled (or unresolved) turbulence energy. This means that the particle-resolved flow contains both the mean flow and the majority of the turbulence, which is generally three-dimensional. A full 3-D SPH–LES model will be expected to provide the accurate flow predictions. However, we must point out that this numerical model is computationally demanding. If we would like to carry out the 3-D simulations, at least 20 particles should be placed in the transverse direction in order to eliminate the influences from the boundaries. This could lead to significant increase of the CPU time.

On the other hand, in the experiments [22], only two components of the turbulence velocities were measured by LDV and the total turbulence kinetic energy was estimated by the empirical formula $k = (2/3)(\overline{u'^2} + \overline{v'^2})$ following Svendsen [25]. This assumes that the turbulence velocities resemble that in a plane wake, which has not been proven. However, Svendsen [25] has shown that the ratio $k/(\overline{u'^2} + \overline{v'^2})$ does not vary greatly for a number of different shear flows so the errors associated with this approximation is expected to be small. To be consistent with the experiments, in the 2-D SPH–LES computations, the calculated turbulence quantities using Equation (12) are multiplied by a factor of $\frac{4}{3}$ to account for the 3-D turbulence effect. In view of the CPU difficulties involved in the 3-D SPH–LES

computations, we temporarily resort to this semi-empirical procedure to compensate for the lack of turbulence in the transverse direction, the feasibility of which has been partially proved by the physical experiments of Ting and Kirby [22].

Model verifications and result analyses

In this section the comparisons are made between the experimental data and numerical results for the mean free surface displacements and turbulence kinetic energies at the four measuring stations, as shown in Figures 2(a)–(d) and 3(a)–(d), respectively. In the figures, the free surface displacements are normalized by the local time-averaged water depth h and the turbulence quantities are normalized by the time-averaged wave phase velocity $c=\sqrt{gh}$. At each location, the comparison of turbulence quantities is made at the highest elevation below the trough level, where the influence of turbulence is the largest. Thus Figures 2(a)–(d) and 3(a)–(d) correspond to the locations of $(x-x_b)/h_b=3.571,\ 6.494,\ 9.740$ and 16.883 $(y-\bar{\zeta})/h=-0.2867,\ -0.4023,\ -0.3807$ and -0.4556, respectively. Meanwhile the numerical

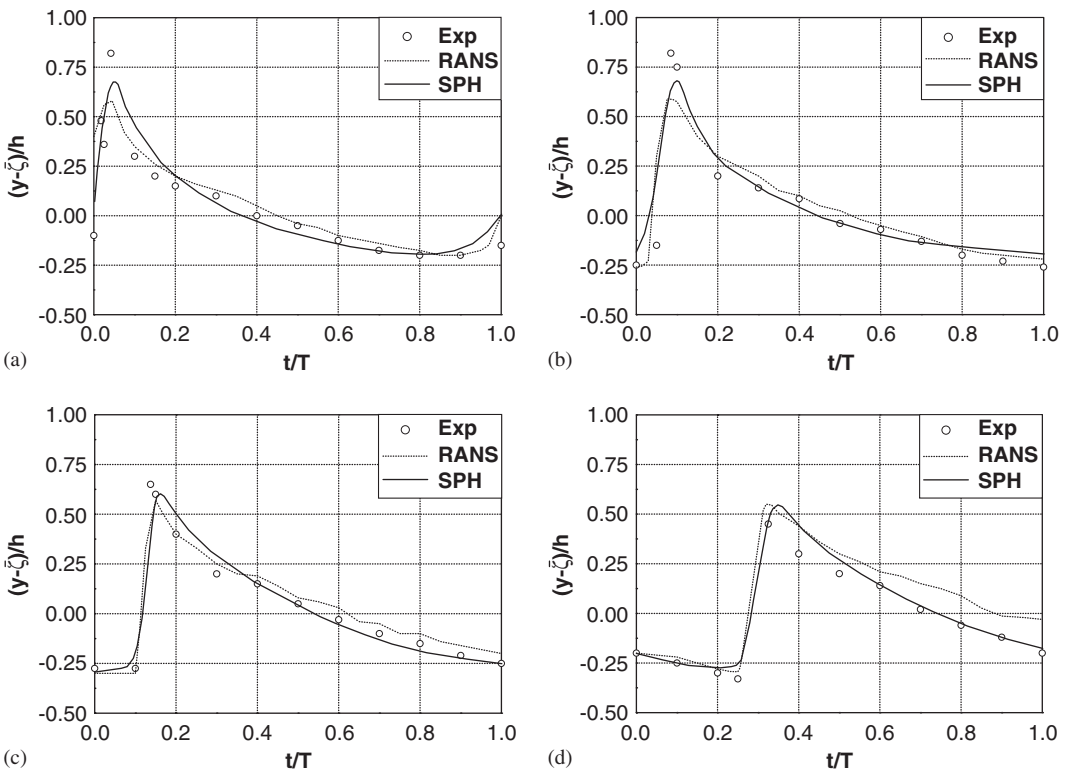

Figure 2. (a)–(d) Computed free surface displacements by SPH–LES model. Compared with experimental data of Ting and Kirby [22] and RANS results of Lin and Liu [2] and comparisons are at locations of $(x-x_b)/h_b$ at: (a) 3.571; (b) 6.494; (c) 9.740; and (d) 16.883.

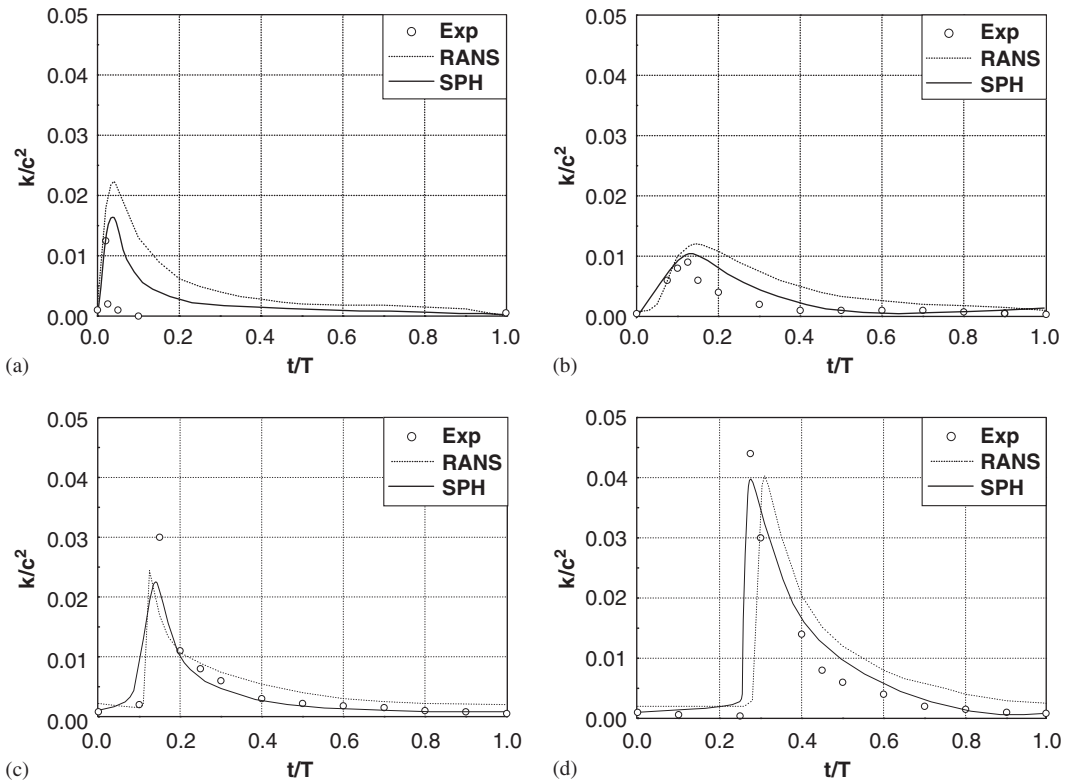

Figure 3. (a)–(d) Computed turbulence intensities by SPH–LES model. Compared with experimental data of Ting and Kirby [22] and RANS results of Lin and Liu [2] and comparisons are at locations of $(x-x_b)/h_b$ and $(y-\overline{\zeta})/h$ at: (a) $(3.571, -0.2867)$; (b) $(6.494, -0.4023)$; (c) $(9.740, -0.3807)$; and (d) $(16.883, -0.4556)$.

results of Lin and Liu [2] by using an RANS approach with the k–ε turbulence modelling are also shown for a comparison. Here it should be noted that the experimental data [22] and the RANS results [2] presented in the figures were actually taken from the paper of Lin and Liu [2] and thereby the present plotting resolutions must be lower than their original ones.

Figures 2(a) and 3(a) show the comparisons at $(x - x_b)/h_b = 3.571$ and $(y - \overline{\zeta})/h = -0.2867$, which is the measuring station closest to the wave breaking point. It is found that the numerical results of Lin and Liu [2] overestimate the turbulence levels and result in excessive energy dissipations, producing a lower surface profile as compared with the experiment. According to Lin and Liu [2], the source of discrepancy could be traced to the use of constant coefficients in the k–ε model. These coefficients have been derived from the quasi-steady flows and may behave poorly in a strongly transient turbulence flow such as the initial breaking wave. Similar problems were also reported in a spilling wave breaking [7], where the numerical model tended to predict an earlier wave breaking point and overestimated the turbulence levels during the initial breaking process. In comparison, the SPH–LES computations predict both the free surface and the turbulence level in a very

satisfactory way. The primary reason is that the SPH model tracks the free surface using particles without the numerical diffusion and thus it can well represent the physical wave hydrodynamics. The particle modelling is capable of capturing the details of small overturning jet at the breaking point [20], which is the major source of turbulence. As a result, it can realistically handle the turbulence generation during this period of time. Besides, the turbulence intensities were calculated based on the phase-averaging of wave series, which is consistent with the physical experiment in interpreting the data. However, both the SPH and RANS computations of Lin and Liu [2] failed to detect a small secondary crest in the surface profile as found in the experiment [22], which could be attributed to the insufficient spatial resolutions. Ting and Kirby [22] reported that the plunging point is slightly seaward of the measuring station and the impact of jet pushes up a wedge of water to form a new wave. Both the new wave and the original wave are clearly seen in the experimental data. The turbulence intensity is highest in the jet and declines rapidly after the passage of the jet. By performing a refined computation of the plunging waves in a constant depth, Lin and Liu [2] confirmed that the turbulence is almost instantaneously generated under the plunging jet when the impingement occurs. This will also be supported by a refined SPH simulation presented in the later section, where a finer particle spacing $\Delta X = 0.013$ m is used.

Figures 2(b) and 3(b) show the comparisons at $(x - x_b)/h_b = 6.494$ and $(y - \bar{\zeta})/h = -0.4023$, respectively. From the experimental data, we can see that the secondary wave caused by the plunging jet has already disappeared and the general turbulence strength has increased. Both the experimental and numerical results indicate that the turbulence distribution is correlated to the primary wave with a slight time delay. This is in sharp contrast with Figures 2(a) and 3(a), in which the turbulence distribution is correlated to the secondary wave generated by the plunging jet. This means that the turbulence generation correlated to the primary wave is the main source in the wave breaking process, which is much stronger than the turbulence generated in the initial plunging. Besides, Figures 2(b) and 3(b) also show that the turbulence intensities vary greatly over one wave cycle. The turbulence level is the highest under the wave front and decays rapidly after the wave crest passes by. This is an indication of a turbulence decay time that is small as compared to the wave period.

Figures 2(c)–(d) and 3(c)–(d) show the comparisons at $(x - x_b)/h_b = 9.740$ and 16.883 and $(y - \bar{\zeta})/h = -0.3807$ and -0.4556, respectively. With the establishment of quasi-steady bore at these two stations, the small-scale motions associated with the initial plunging jet disappear and the mean flow is smooth enough to be solved by the current mesh resolutions. Thus the numerical results from two different models agree with the experimental wave profiles and turbulence intensities much better than the comparisons in the previous two stations. Furthermore, the influence of different turbulence modelling approaches, such as the LES model (in the SPH) or k–ε model (in the RANS [2]), is becoming less important. This is manifested by the close agreement of two numerical turbulence intensity profiles as shown in the figures. The turbulence level is still higher than that in the previous locations and it spreads out over a longer duration as the bore moves forward. According to Ting and Kirby [22], the ratio of wave height to local water depth reaches a quasi-constant value of 0.8 in the inner surf zone, which is considerably larger than the value of 0.5 for a spilling breaker.

The spatial evolution features of the breaking wave will be shown in Appendix A based on the refined SPH–LES computations using a particle spacing $\Delta X = 0.013$ m.

SENSITIVITY ANALYSES OF SPH–LES MODEL

Influence of particle spacing on numerical results

Although the SPH method has been extensively applied in many areas, there are still a lot of issues that need to be further addressed. One of them is the analysis of numerical accuracy dependent on the spatial resolution. In some simple cases, it is possible to perform the theoretical analysis of the SPH numerical schemes [18]. However, in the present long-time wave breaking simulations, in which the fluid particles are highly disordered, the analysis of numerical accuracy can only be achieved through the numerical tests. Here, the numerical tests also aim to estimate the accuracy of computed turbulence quantities based on the phase-averaging approach. In the previous computations, a relatively coarse particle spacing $\Delta X = 0.02$ m was used, so there are some details of the turbulence which were not resolved by the model. In order to quantitatively investigate the sensitivity of the model to the particle spacing ΔX, an additional numerical run is implemented with the particle numbers being doubled and thus the particle spacing is reduced to $\Delta X = 0.013$ m. Since different problem setups can introduce difference in the results and the role of mesh change could become unclear, the location of the wave paddle and the number of waves being phase-averaged in the refined computation are kept the same as those in the previous coarse computation. There are about 20 000 particles involved in the refined simulations. The computations are executed to $t = 70T$ with the last 60 waves being used for phase-averaging.

The computed free surface displacements using both the coarse and refined particle spacing, i.e. $\Delta X = 0.02$ and 0.013 m, are shown in Figures 4(a)–(d) at the four measuring stations. Inside the figures, the experimental data of Ting and Kirby [22] are also shown for a comparison. It is very obvious that as the particle spacing ΔX becomes smaller, the computed curves match the experiment better. Especially, the refined SPH computations disclose the secondary wave in the surface profile as shown in Figure 4(a), which was generated by the plunging jet impingement and not found in the coarse SPH computations.

Another purpose of making the refined SPH computations is to quantitatively investigate the influences of sub-particle scale (SPS) turbulence under a prevailing particle spacing ΔX. For this, the total turbulence kinetic energy k and the SPS turbulence energy k_{SPS} are also plotted together with the experimental data in Figures 5(a)–(d), for both the coarse and refined computations. It is shown that the variation of SPS turbulence over one wave cycle is much milder than that of the total (or phase-averaged particle scale) turbulence and the SPS turbulence profile is closely correlated with the total turbulence profile. The contribution of SPS turbulence is around 20% for the computations using a particle spacing $\Delta X = 0.02$ m. However, as the particle spacing is reduced to $\Delta X = 0.013$ m, the contribution of SPS turbulence becomes much smaller and consists of only 10% of the total turbulence. The decreasing rate of turbulence is proportional to $O(\Delta X^2)$, which is due to that the turbulence is calculated as the square of velocity fluctuations and the global accuracy of the SPH numerical scheme is around $O(\Delta X)$ [19]. The findings are consistent with the fundamental LES theory in that as the grid size becomes smaller, more turbulence can be directly resolved by the fluctuations of the velocities and the phase-averaged turbulence intensities should approach the real turbulence levels.

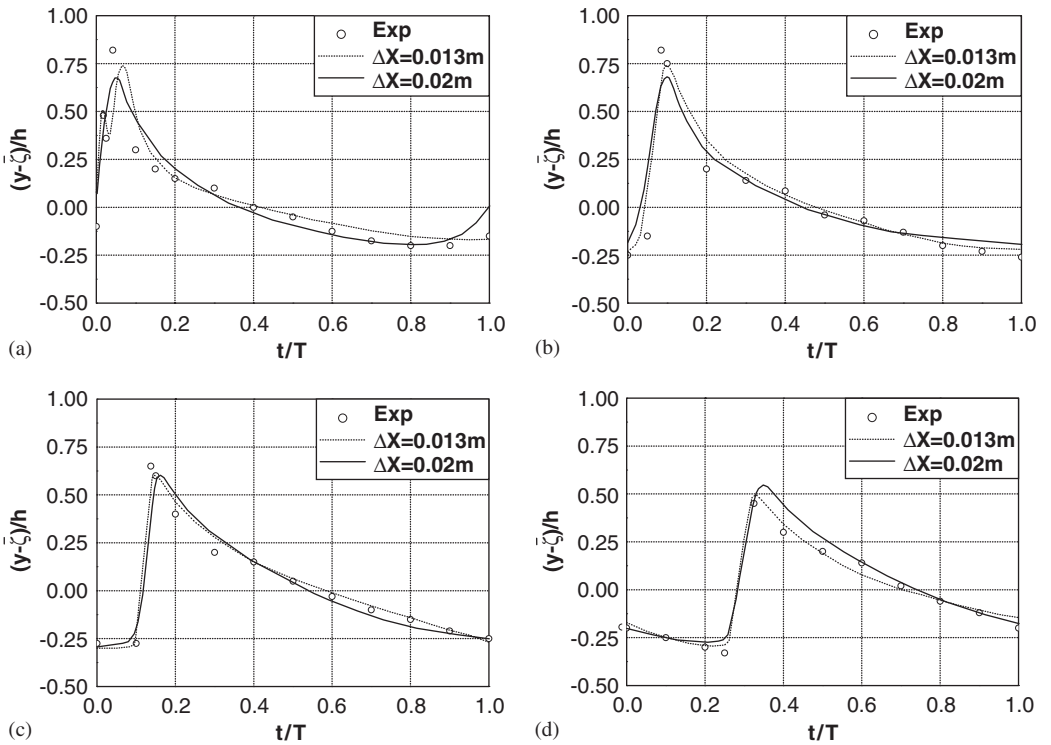

Figure 4. (a)–(d) Computed free surface displacements by SPH–LES model using particle spacing $\Delta X = 0.02$ and 0.013 m. Compared with experimental data of Ting and Kirby [22] and comparisons are at locations of $(x - x_b)/h_b$ at: (a) 3.571; (b) 6.494; (c) 9.740; and (d) 16.883.

Influence of turbulence modelling on numerical results

In order to study the influence of turbulence modelling on the wave breaking simulations, the SPH–LES model is first run without the LES–SPS turbulence model by setting the Smagorinsky constant $C_s = 0.0$, meanwhile the other parameters are kept unchanged. The computed free surface profiles and phase-averaged particle scale (PS) turbulence kinetic energies at the four measuring stations are shown in Figures 6(a)–(d) and 7(a)–(d), respectively, compared with the numerical results obtained with the turbulence modelling and the experimental data of Ting and Kirby [22]. It is shown from Figure 6 that the computed surface profiles without the turbulence modelling produce relatively larger wave height due to the lack of turbulence dissipation, although the two wave forms are generally similar in the shape and phase. The maximum difference in the computed wave height from two different numerical runs is around 10–15%, which appears at the first measuring station closest to the wave breaking point. Besides, it is also found from Figure 7 that the phase-averaged PS turbulence intensities increase by about 20–40% in the non-turbulence computations, which is due to the increase of velocity fluctuations because of the reduction of smoothing mechanism provided by the turbulence diffusion. In contrast to the wave surface profiles, the minimum difference

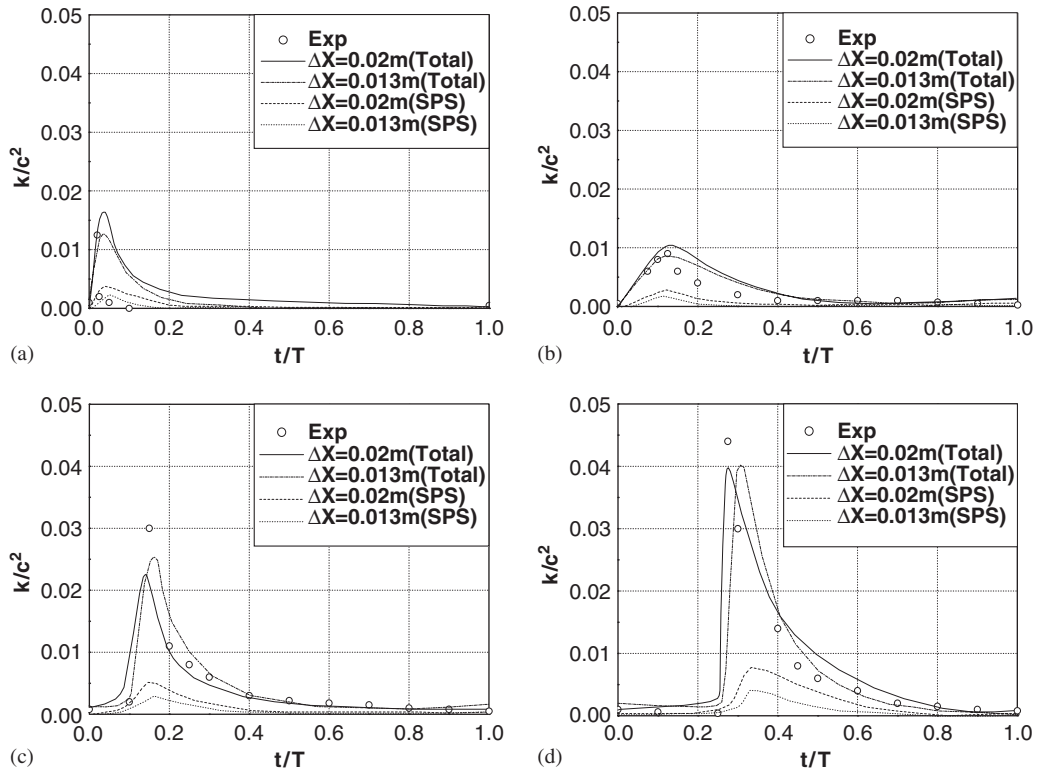

Figure 5. (a)–(d) Computed total and sub-particle scale (SPS) turbulence intensities by SPH–LES model using particle spacing $\Delta X = 0.02$ and 0.013 m. Compared with experimental data of Ting and Kirby [22] and comparisons are at locations of $(x-x_b)/h_b$ and $(y-\overline{\zeta})/h$ at: (a) $(3.571, -0.2867)$; (b) $(6.494, -0.4023)$; (c) $(9.740, -0.3807)$; and (d) $(16.883, -0.4556)$.

in the computed PS turbulence intensities by the two runs is observed at the first measuring station. In all the cases shown in Figure 7, both of the PS turbulence curves cannot agree reasonably with the experiment due to the exclusion of SPS turbulence arising from the insufficient mesh resolutions. The above comparisons indicate that the turbulence modelling is indispensable for the accurate simulation of the plunging waves, since the turbulence produced by the violent overturning jet is quite strong and thus has a profound influence on the mean flow fields. However, after the local wave breaking process has passed and the resulting turbulent bore has started to propagate in the onshore direction, the small-scale effect of the overturning jet is no longer dominant and the influence of turbulence on the mean flow fields becomes less important. Thus we could anticipate that the flow can be reasonably solved by using a constant viscosity without the need to use a turbulence model.

To further investigate the influence of different turbulence modelling approaches on the computed results, another SPH run is carried out, in which the two-equation k–ε model is used as the turbulent closure. The detailed descriptions and formulations of the coupled SPH

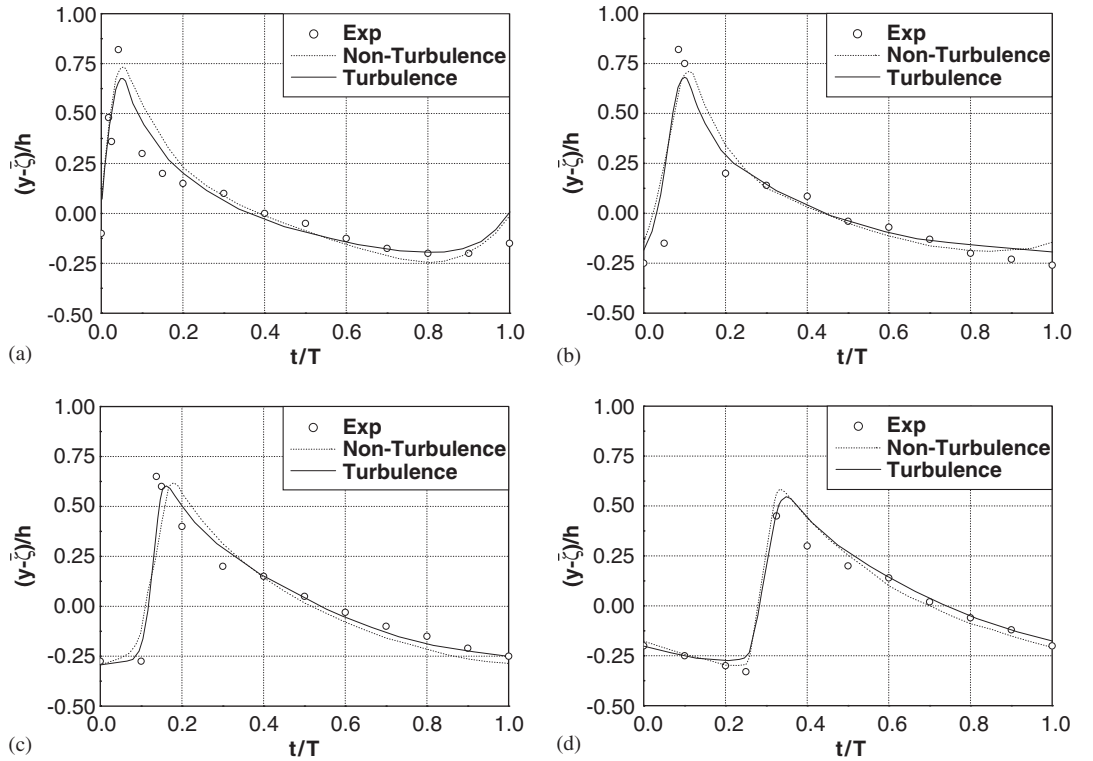

Figure 6. (a)–(d) Computed free surface displacements by SPH model with and without LES turbulence modelling. Compared with experimental data of Ting and Kirby [22] and comparisons are at locations of $(x - x_b)/h_b$ at: (a) 3.571; (b) 6.494; (c) 9.740; and (d) 16.883.

and k–ε model can be found in References [20, 21]. Here a brief review is given: In the SPH—k–ε model, additional two transport equations for the turbulence production k and the dissipation rate ε are solved using the SPH particle approach. The turbulence quantities are updated after the mean flow fields are obtained. On the free surface, the zero-gradient boundary conditions are imposed to both the k and ε to ensure their advective and diffusive fluxes to be zero. Thus there is no turbulence exchange between the air and water. Besides, the widely used log-law distribution is employed for the turbulence conditions near the solid boundary. For the k–ε model, it is also necessary to seed a small amount of k and ε into the initial and inflow boundary conditions. It is found that the final computational results are relatively insensitive to the initial seeding. In this paper, we assume that the initial condition should be described in such a way to satisfy $\nu_T = \nu_0$, while at the inflow boundary $\nu_T = 10\nu_0$ should be applied. The similar seeding values of k and ε in References [20, 21] are used, which assume that the initial turbulence level is quite low in the inner fluid region and slightly higher near the inflow boundary.

To be consistent with Lin and Liu [2], in which the numerical results over one wave period from $t = 17.4$ to 22.4 s were used, the numerical data of the 4th wave computed by the SPH model are used here for comparison with the experiments and the results of Lin and Liu. Due

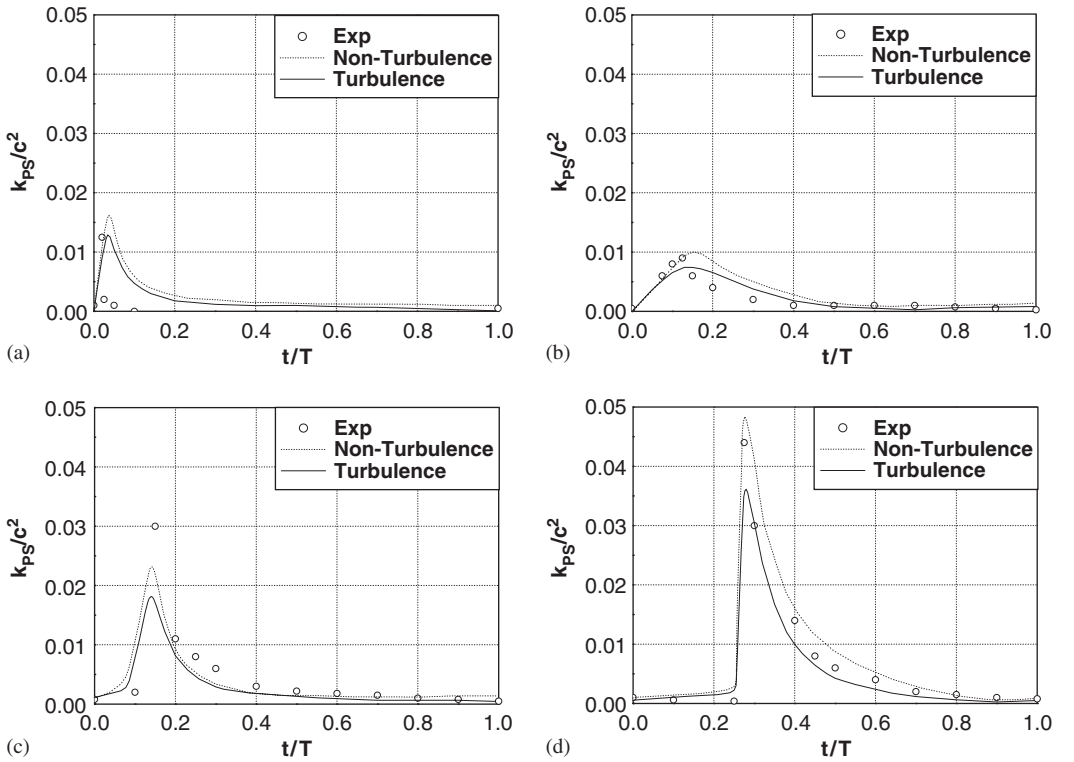

Figure 7. (a)–(d) Computed particle scale (PS) turbulence intensities by SPH model with and without LES turbulence modelling. Compared with experimental data of Ting and Kirby [22] and comparisons are at locations of $(x-x_b)/h_b$ and $(y-\bar{\zeta})/h$ at: (a) $(3.571, -0.2867)$; (b) $(6.494, -0.4023)$; (c) $(9.740, -0.3807)$; and (d) $(16.883, -0.4556)$.

to the increase of computational load arising from the solutions of two transport equations, we have not tried to make a detailed analysis on the sensitivity of computations, such as the difference between two consecutive waves and the influence of mesh refinements.

According to the SPH—k–ε computations, the computed turbulence intensities at the four measuring stations are shown in Figures 8(a)–(d), respectively, compared with the numerical results of Lin and Liu [2] using a RANS model with the non-linear k–ε turbulent closure and the experimental data of Ting and Kirby [22]. It is quite interesting to see that the computed turbulence profiles by the SPH model are very close to those predicted by Lin and Liu [2] in all the cases. Especially, both numerical models significantly overestimate the turbulence levels at the first measuring station, where the production of turbulence is at the early stage. Figure 8 provides quantitative support to the comments made by Lin and Liu [2, 7] and Christensen *et al.* [9] that the overestimation of turbulence levels in the surf zone could be partly attributed to the employment of different turbulence models.

Finally, we must realize that both the SPH and RANS results presented in Figure 8 were obtained by using a particular wave. At this time, according to the graphic analysis of the SPH particle snapshots, the computed waves in the surf zone have not reached the quasi-steady

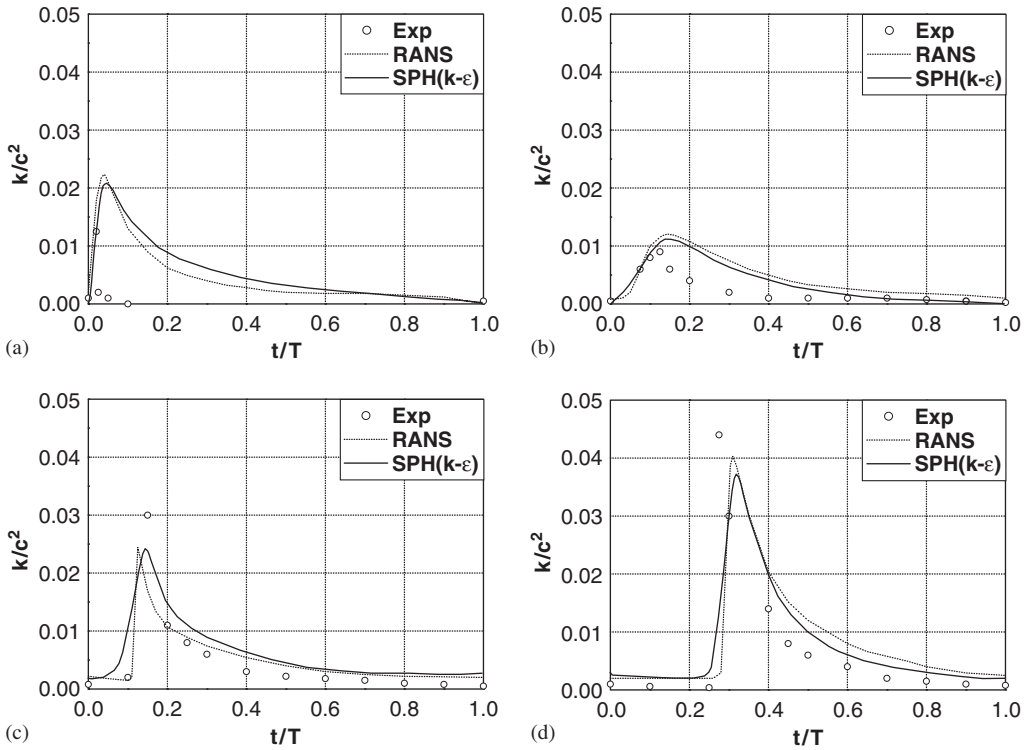

Figure 8. (a)–(d) Computed turbulence intensities by SPH—k–ε model. Compared with experimental data of Ting and Kirby [22] and RANS results of Lin and Liu [2] and comparisons are at locations of $(x-x_b)/h_b$ and $(y-\overline{\zeta})/h$ at: (a) $(3.571, -0.2867)$; (b) $(6.494, -0.4023)$; (c) $(9.740, -0.3807)$; and (d) $(16.883, -0.4556)$.

state and the full set-ups and set-downs have not achieved. If the present model and the RANS model of Lin and Liu [2, 7] could be run for a much longer time scale and the numerical results could be interpreted by averaging a lot of wave series, the prediction of turbulence quantities should be expected to be accurate even if the two-equation k–ε model is employed as the turbulent closure.

CONCLUSIONS AND DISCUSSIONS

The paper presents the SPH with 2-D LES modelling approach to investigate a plunging wave breaking case. The computations are in good agreement with the documented data. The SPH method is shown to be effective in describing the free surfaces of large deformation in the surf zone. The sub-particle scale (SPS) turbulence model is proved to be capable of adequately predicting the turbulence levels under the breaking waves following a phase-averaging approach. The numerical results are found to be better than those obtained by using a RANS model in the tested range. The sensitivity analysis of the model indicates that more

turbulence can be directly resolved by using a refined spatial resolution and the contributions from the SPS turbulence become less important at a finer particle size.

The present SPH–LES model gave satisfactory results of turbulence under the breaking waves, which could be mainly attributed to the robustness of the SPS turbulence model. Since the spatial resolution (or particle size) is not fine enough to perform the direct numerical simulation, the turbulence quantities must be calculated by means of a modelling approach. The traditional turbulent closures such as the two equation k–ε model, is incapable of accurately predicting the initiation of turbulence during the early stage of wave breaking, due to several reasons as explained by Lin and Liu [2, 7] and Christensen *et al.* [9]. For example, the k–ε model cannot accurately address the initiation of turbulence in a rapidly distorted shear flow region such as in the wave breaking. Besides, the uncertainties in the initial and inflow boundary conditions for the turbulence kinetic energy also introduce difficulties for the k–ε model to predict the exact wave breaking point. The findings in this paper further disclose the importance of the SPS turbulence, which arises from the lack of high spatial resolutions. Here it is worth noticing that the RANS results were obtained by using a particular wave rather than an average of many wave series. The phase-averaging approach in the SPH computations improved the accuracy of model predictions and reduced the numerical errors, but at the sacrifice of CPU time. Computationally, the SPH–LES model has the advantage in that the computational load is reduced since there is no need to solve two additional transport equations.

In future work, a two-phase SPH model should be established to account for the influence of air entrainments during the wave breaking. In addition, a full 3-D SPH–LES model is expected to accurately predict the turbulence levels under the breaking waves. However, this numerical model is computationally demanding (for example, a 50% mesh refinement could require about 16-fold increase of CPU time). Therefore, the parallelization of the SPH code is also an important task.

APPENDIX A: SPATIAL EVOLUTION FEATURES OF BREAKING WAVE

One of the great advantages of the numerical model is its ability to disclose the distributions of relevant physical properties in the spatial and temporal domains. Based on the refined SPH–LES computations using a particle spacing $\Delta X = 0.013$m with about 20 000 particles, the particle snapshots, velocity fields and turbulence eddy viscosity distributions of the breaking wave are shown in Figures A1(a)–(c), A2(a)–(c) and A3(a)–(c), respectively. It is shown that the general features of the wave breaking, collapsing and subsequent turbulent bore formation have been well captured by the SPH–LES computations. The simulated wave breaking patterns are consistent with the numerical predictions by Lin and Liu [2] and Bradford [8] and the laboratory observations by Ting and Kirby [22].

The plunging wave breaking is a quite violent event and the waves deform drastically as shown in Figures A1(a)–(c). The overturning of wave front at the breaking is adequately disclosed by the SPH computations in Figure A1(b). The curling forward of wave crest hits the surface of wave trough and the impact of jet pushes up a wedge of water to form a new wave in Figure A1(c). By investigating the velocity fields in Figures A2(a)–(c), it is shown that the velocity distributions of the plunging wave deviate significantly from the linear wave theory and the magnitude of velocity is rather large. As seen in Figure A2(b),

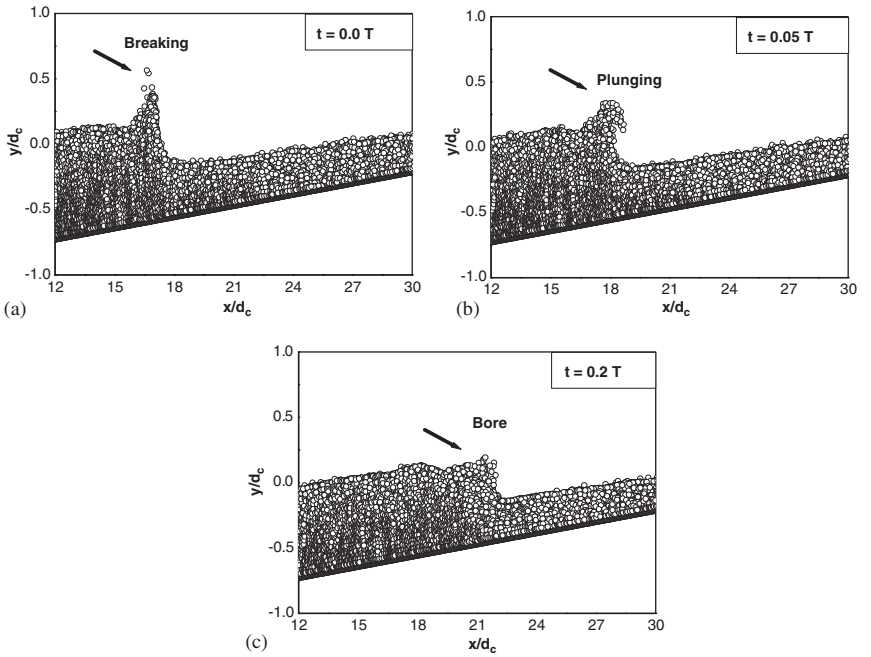

Figure A1. (a)–(c) Particle snapshots during wave breaking, plunging and turbulent bore formation.

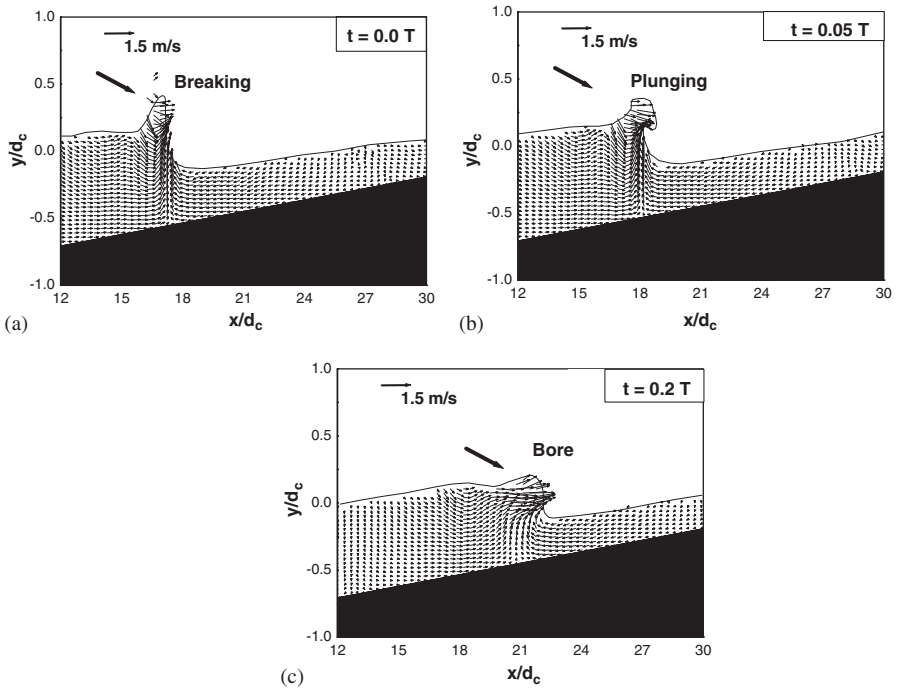

Figure A2. (a)–(c) Velocity fields during wave breaking, plunging and turbulent bore formation.

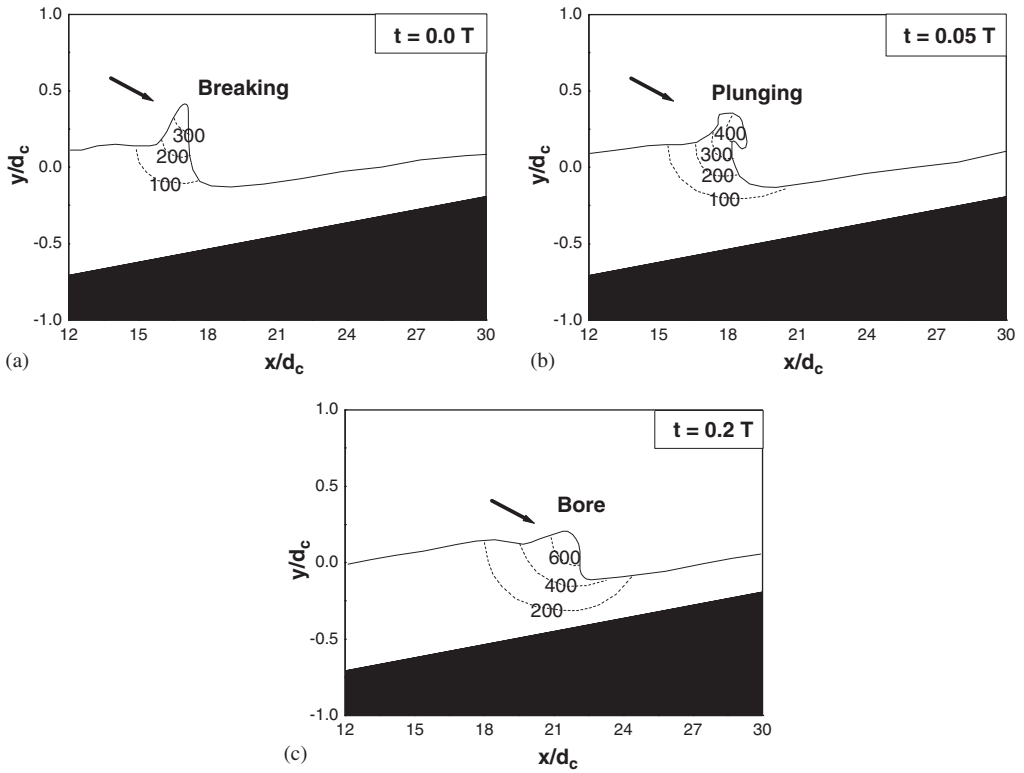

Figure A3. (a)–(c) Turbulence eddy viscosities (v_T/v_0) during wave breaking, plunging and turbulent bore formation.

the plunging jet with a maximum velocity of 2.0 m/s plunges towards the wave trough and the impact generates a turbulent bore with a velocity of 2.5 m/s in Figure A2(c). The velocity structures immediately underneath the wave trough at the impingement are greatly modified by the penetration of the plunging jet. This indicates that the plunging wave has an obvious transitional stage, in which the wave rapidly changes the shape and dissipates the energy.

By means of the LES–SPS turbulence modelling, the turbulence eddy viscosity distributions are shown in Figures A3(a)–(c). According to Gotoh *et al.* [15], the eddy viscosity v_T is a good representation of turbulence levels in the study of the breaking waves. In the figures, the eddy viscosity is normalized by the laminar viscosity value v_0. It is shown that the turbulence levels increase rapidly after the wave breaking. The maximum turbulence as represented by the contour of $v_T/v_0 = 600$ is generated instantaneously as the plunging jet touches down on the wave trough in Figure A3(b). The roller continues to spread downwards as the breaking wave front propagates downstream and can penetrate as deep as half of the water depth, as found in Figure A3(c). However, our computations indicate that the initial geometry and strength of the plunging jet only have the local influence on the wave motion

and have little impact on the turbulence transport mechanisms a short distance away from the plunging point.

APPENDIX B: NOMENCLATURE

c	wave celerity
C_s	Smagorinsky constant
C_T	turbulence constant
d	local still water depth
d_0	still water depth at the original
d_c	constant water depth
$\mathbf{g}$	gravitational acceleration
h	kernel smoothing distance or time-averaged water depth
h_b	water depth at wave breaking point
H	wave height
k	turbulence kinetic energy
k_{PS}	particle scale (PS) turbulence kinetic energy
k_{SPS}	sub-particle scale (SPS) turbulence kinetic energy
m	particle mass
P	pressure
$\mathbf{r}$	position vector
s	slope of beach
$\lvert\overline{S}\rvert$	local shear rate
$\overline{S}_{ij}$	strain rate of mean flow
t	time
T	wave period
$u(v)$	instantaneous velocities
$\overline{u}(\overline{v})$	mean velocities
$u'(v')$	turbulence velocities
$\mathbf{u}$	velocity vector
$W(\nabla_a W_{ab})$	interpolation kernel and gradient of the kernel
x	horizontal coordinate
x_b	location of wave breaking point
y	vertical coordinate
δ_{ij}	Kronecker delta
Δt	time increment
ΔX	particle spacing
ε	turbulence dissipation rate
ζ	instantaneous water surface
$\overline{\zeta}$	time-averaged water surface
ν_0	kinetic viscosity of laminar flow
ν_T	turbulence eddy viscosity
ρ	fluid density
$\overrightarrow{\overrightarrow{\boldsymbol{\tau}}}$	sub-particle scale (SPS) stress tensor
τ_{ij}	element of stress tensor

Subscripts and symbols

a reference particle
b neighbouring particle

ACKNOWLEDGEMENTS

The incompressible SPH code in the paper was developed and improved from the Moving Particle Semi-implicit (MPS) program provided by Professor Seiichi Koshizuka, The University of Tokyo. The authors are very grateful to Professor Hitoshi Gotoh at Kyoto University, Professor Pengzhi Lin at National University of Singapore, Professor Edmond Yat-man Lo and Professor Niansheng Cheng at Nanyang Technological University for their constructive ideas and guidance on the SPH and LES turbulence modelling.

The paper is supported by the National Natural Science Foundation of China (Grant number 50579019).

REFERENCES

1. Dean RG, Dalrymple RA. *Water Wave Mechanics for Engineers and Scientists*. Advanced Series on Ocean Engineering, vol. 2. World Scientific Publication: Singapore, 1991.
2. Lin PZ, Liu PLF. Turbulence transport, vorticity dynamics, and solute mixing under plunging breaking waves in surf zone. *Journal of Geophysical Research* 1998; **103**(C8):15677–15694.
3. Grilli ST, Subramanya R, Svendsen IA, Veeramony J. Shoaling of solitary waves on plane beaches. *Journal of Waterway, Port, Coastal and Ocean Engineering* (ASCE) 1994; **120**(6):609–628.
4. Zelt JA. The run-up of nonbreaking and breaking solitary waves. *Coastal Engineering* 1991; **15**:205–246.
5. Lemos C. *Wave Breaking, A Numerical Study*. Lecture Notes in Engineering, vol. 71. Springer: Berlin, 1992.
6. Takikawa K, Yamada F, Matsumoto K. Internal characteristics and numerical analysis of plunging breaker on a slope. *Coastal Engineering* 1997; **31**(1–4):143–161.
7. Lin PZ, Liu PLF. A numerical study of breaking waves in the surf zone. *Journal of Fluid Mechanics* 1998; **359**:239–264.
8. Bradford SF. Numerical simulation of surf zone dynamics. *Journal of Waterway, Port, Coastal and Ocean Engineering* (ASCE) 2000; **126**(1):1–13.
9. Christensen ED, Walstra DJ, Emerat N. Vertical variation of the flow across the surf zone. *Coastal Engineering* 2002; **45**(3&4):169–198.
10. Lin PZ, Liu PLF. Discussion of 'Vertical variation of the flow across the surf zone'. *Coastal Engineering* 2004; **50**:161–164.
11. Watanabe Y, Saeki H. Three-dimensional large eddy simulation of breaking waves. *Coastal Engineering Journal* 1999; **41**(3&4):281–301.
12. Christensen ED, Deigaard R. Large eddy simulation of breaking waves. *Coastal Engineering* 2001; **42**(1):53–86.
13. Smagorinsky J. General circulation experiments with the primitive equations, I. The basic experiment. *Monthly Weather Review* 1963; **91**:99–164.
14. Zhao Q, Tanimoto K. Numerical simulation of breaking waves by large eddy simulation and VOF-method. *Proceedings of 26th International Conference on Coastal Engineering* (*ICCE*), Copenhagen, Denmark, vol. 1, 1998; 892–905.
15. Gotoh H, Shibahara T, Sakai T. Sub-particle-scale turbulence model for the MPS method—Lagrangian flow model for hydraulic engineering. *Computational Fluid Dynamics Journal* 2001; **9**(4):339–347.
16. Koshizuka S, Tamako H, Oka Y. A particle method for incompressible viscous flow with fluid fragmentation. *Computational Fluid Dynamics Journal* 1995; **4**:29–46.
17. Monaghan JJ. Smoothed particle hydrodynamics. *Annual Review of Astronomy and Astrophysics* 1992; **30**:543–574.
18. Monaghan JJ, Kos A. Solitary waves on a cretan beach. *Journal of Waterway, Port, Coastal and Ocean Engineering* (*ASCE*) 1999; **125**(3):145–154.
19. Shao SD, Gotoh H. Turbulence particle models for tracking free surfaces. *Journal of Hydraulic Research* 2005; **43**(3):276–289.
20. Shao SD. Simulation of breaking wave by SPH method coupled with k–ε model. *Journal of Hydraulic Research* 2005, in press.
21. Shao SD. Incompressible SPH simulation of wave breaking and overtopping with turbulence modelling. *International Journal for Numerical Methods in Fluids* 2006, in press.

22. Ting FCK, Kirby JT. Dynamics of surf-zone turbulence in a strong plunging breaker. *Coastal Engineering* 1995; **24**:177–204.
23. Yoshizawa A. Eddy-viscosity-type subgrid-scale model with a variable Smagorinsky constant and its relationship with the one-equation model in large eddy simulation. *Physics of Fluids* 1991; **A3**(8):2007–2009.
24. Christensen ED, Walstra DJ, Emerat N. Reply to discussion of 'Vertical variation of the flow across the surf zone'. *Coastal Engineering* 2004; **50**:165–166.
25. Svendsen IA. Analysis of surf zone turbulence. *Journal of Geophysical Research* 1987; **92**(C5):5115–5124.

